Appl. Phys. A 68, 9–18 (1999)

Applied Physics A
Materials
Science & Processing

Dopant diffusion and segregation in semiconductor heterostructures: Part 1. Zn and Be in III-V compound superlattices

C.-H. Chen, U.M. Gösele, T.Y. Tan*

Department of Mechanical Engineering and Materials Science, Duke University, Durham, NC 27708-0300, USA

Received: 20 August 1998/Accepted: 23 September 1998

Abstract. Distribution of shallow dopants in semiconductor heterostructures in general exhibits a pronounced segregation phenomenon, which requires the description of the dopant atom diffusion and segregation processes simultaneously. We treat this class of problems in a series of three papers. In the present paper, which is the first of the three, Zn and Be distributions in III-V superlattice (SL) structures are discussed in detail. The analysis method developed in this paper is generally applicable to other cases. In the second paper we analyze B distribution in GeSi/Si heterostructures. In the third paper we treat the problems associated with a number of n-type dopants in a variety of semiconductor heterostructures. Segregation of a dopant species between two semiconductor heterostructure layers is explained by a model incorporating (i) a *chemical* effect on the neutral species; and (ii) a *Fermi-level* effect on the ionized species, because, in addition to the chemical effect, the solubility of the species also has a dependence on the semiconductor Fermi-level position. For Zn and Be in GaAs and related compounds, their diffusion process is governed by the doubly-positively-charged group III element self-interstitials (I_{III}^{2+}), whose thermal equilibrium concentration, and hence also the diffusivity of Zn and Be, exhibit also a Fermi-level dependence, i.e., in proportion to p^2. A heterojunction consists of a space-charge region with an electric field, in which the hole concentration is different from those in the bulk of either of the two layers forming the junction. This local hole concentration influences the local concentrations of I_{III}^{2+} and of Zn^- or Be^-, which in turn influence the distribution of these ionized acceptor atoms. The process involves diffusion and segregation of holes, I_{III}^{2+}, Zn^-, or Be^-, and an ionized interstitial acceptor species. The junction electric field also changes with time and position.

PACS: 61.72.Vv; 61.72.Ss; 61.72.Yx

Distribution of shallow dopants in semiconductor heterostructures in general exhibits a pronounced segregation phenomenon, which requires the description of the dopant atom diffusion and segregation processes simultaneously. We treat these class of problems in a series of three papers. In this present paper, which is the first part, we present the general method of formulating such problems with an emphasis of application to Zn and Be distributions in III-V superlattice (SL) structures. In the second paper, we analyze B distribution in GeSi/Si heterostructures [1]. In the third paper, we treat the problems associated with a number of n-type dopants in a variety of semiconductor heterostructures [2].

In GaAs and in AlGaAs/GaAs-type superlattices (SL), self-diffusion and diffusion of dopant atoms on the group III sublattice of GaAs and other III-V compound semiconductors are governed by charged point defects [3–6]. In intrinsic and n-type materials, the triply-negatively-charged group III vacancies V_{Ga}^{3-} dominate the diffusion processes of self- and impurity atoms occupying the group III sublattice, for example, Si, whereas in highly doped p-type materials the doubly-positively-charged group III self-interstitials I_{III}^{2+} dominate the group III atom self-diffusion and diffusion of the p-dopant Zn and Be atoms which occupy group III sublattice sites [4–6]. Because the point defect species are charged and hence their thermal equilibrium concentrations are dependent upon the semiconductor doping type and level, the diffusivities of atomic species utilizing the appropriate point defects as diffusion vehicles are also dependent upon the semiconductor doping type and level, which is known as the Fermi-level effect [3–6]. To arrive at these conclusions, in previous analyses [4–6] of dopant and self-atom diffusion profiles in AlGaAs/GaAs SL structures, the effect of the dopant solubility difference in the SL layers has been ignored, which is justifiable for two reasons. First, experimental results showed that the solubility difference of the dopants in AlAs and in GaAs is small. Second, layer disordering has occurred in the experiments which minimizes the effect arisen from the dopant solubility difference.

In fabricating some III-V SL device structures for which the involved acceptor diffusion time is short and/or the diffusion temperature is relatively low, the p-type dopants Zn

* E-mail: ttan@acpub.duke.edu

and Be showed a prominent segregation behavior in the SL layers [7–9]. This segregation phenomenon is caused by the dopant solubility difference in the layers when there is no substantial layer disordering taking place to smooth out the material compositional and chemical differences. In this paper, we describe a detailed quantitative model to account for the dopant SL layer-dependent distribution process, including the segregation phenomenon. The model considers the dopant solubility dependence on the Gibbs free energy of incorporating a neutral dopant atom onto the semiconductor lattice site, which is determined *chemically*, and the concept of the Fermi-level dependence of the ionized shallow dopant solubility. The model also considers the dopant atom diffusion process via the Fermi-level dependence of the governing point defect concentrations, as well as the effect of carrier concentrations at the heterojunctions. A preliminary such study was first carried out by the present authors on III-V compound SL layer disordering due to Si doping [10].

The overall dopant distribution process involves diffusion and segregation of holes, I_{III}^{2+}, Zn^{-}, or Be^{-}, and an ionized interstitial acceptor species. The junction electric field also changes with time and position.

1 The diffusion–segregation equation

Because of the involvement of a large number of species for each of which diffusion and segregation occur simultaneously, the diffusion–segregation equation derived by You et al. [11],

$$\frac{\partial C}{\partial t} = \frac{\partial}{\partial x}\left[D\left(\frac{\partial C}{\partial x} - \frac{C}{C^{\mathrm{eq}}}\frac{\partial C^{\mathrm{eq}}}{\partial x} \right) \right] , \tag{1}$$

is used to formulate the problem. In (1) C^{eq} denotes the thermal equilibrium concentration or solubility of the considered species at the given temperature. The second term on the right-hand side (RHS) of (1) accounts for the spatial variations in C^{eq} due to any physical cause, but not including that of a temperature gradient.

2 Charged point defect thermal equilibrium concentrations

For III-V compounds and especially for GaAs and AlAs, it is well recognized that the Fermi level plays the eminent role in leading to the charge dependence of the dopant diffusivities via its effect on the concentrations of charged point defects which govern the dopant diffusion processes [3–6]. This is one effect of the Fermi level, for which the position of the Fermi level is determined by a shallow dopant species. The energy level positions of the involved charged point defect species are assumed to be deep in the semiconductor band gap and hence the concentrations of the defects are small so that they do not have a noticeable influence on the Fermi level position determined by the shallow dopants. The Fermi-level dependence of the thermal equilibrium concentrations of charged point defects has been discussed elsewhere in detail [4–6], and in the present paper we will use this knowledge.

3 Shallow acceptor solubilities

In this section, we discuss the solubility issue encountered for shallow acceptor species. It is noted, however, that the general principle applies also to shallow donor species.

A shallow acceptor species in a semiconductor at a given temperature consists of a neutral and an ionized species. The Fermi level affects the solubilities of the ionized shallow acceptor species A^{-}. Since the semiconductor Fermi level is in turn determined by shallow dopants, we see that there is a mutual dependence of the Fermi level and the dopant solubility. We need to consider the ionized dopant solubilities because we will use the diffusion segregation equation of You et al. [11], (1), to formulate the present problem.

It is standard textbook knowledge that, at a given temperature, in the presence of one and only one kind shallow dopant of a given total concentration, the partition between the ionized and neutral species is according to the Fermi–Dirac distribution function. This is a *closed* thermodynamic system containing the semiconductor crystal and the dopant of the given total concentration. Under the closed-system constraint that the total dopant concentration is constant, this partitioning is the consequence of the fact that the free energy of this closed system is minimized. In this sense, the concentrations of both the neutral and ionized dopant species are those under thermal equilibrium conditions. However, the ratio of the so-partitioned values will change with a change in the total dopant concentrations which in practice can be largely varied. Thus, these closed-system equilibrium quantities cannot be defined as the solubilities of the appropriate species.

At a given temperature, a *unique* thermal equilibrium concentration or solubility value of the neutral, the ionized, and the total dopant species is defined for the semiconductor crystal which is *open* to a unique dopant source material. This dopant source material is the one and only one in thermal equilibrium coexistence with the semiconductor crystal containing dopant atoms, which is a compound phase composed of the dopant element and elements constituting the semiconductor crystal, but not any other elements. If, by some means, the total dopant concentration introduced into the semiconductor is below the appropriate solubility value, subsequently the closed-system equilibrium conditions apply and the dopant atoms will be partitioned accordingly. If, instead, the total dopant concentration introduced into the semiconductor is above the appropriate solubility value, the subsequent *thermal equilibrium* process will result in that, in the semiconductor matrix material, dopant atoms will reach the solubility values of the neutral and ionized species and simultaneously precipitates of the unique source material phase, which determines the dissolved species solubility values, form. Figure 1 schematically illustrates the situations discussed above.

The effect of the Fermi level on the solubilities of the ionized shallow donors D^{+} or acceptors A^{-} has only been scarcely addressed. In fact, we are aware of only one discussion on this issue that is sufficiently explicit and fundamental. Using a thermodynamic formulation, Yu et al. [12] showed that, for Zn^{-} or Be^{-} in GaAs, the solubility of the ionized acceptor species $C_{\mathrm{A}^{-}}^{\mathrm{eq}}$ is proportional to $1/p$, where p is the hole concentration in the crystal. The value of $C_{\mathrm{A}^{-}}^{\mathrm{eq}}$ is also

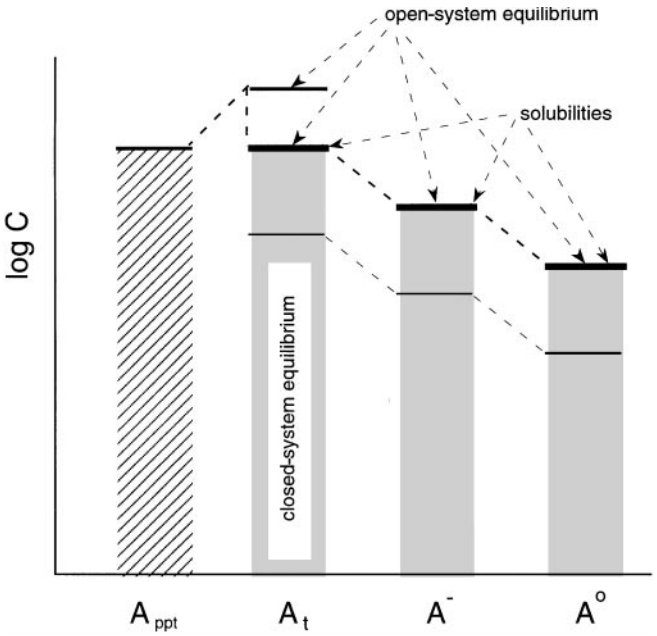

Fig. 1. A schematic diagram showing the solubility values of the neutral, the ionized, and the total concentrations of a shallow dopant species in a semiconductor, which is defined in an *open* system consisting also of the dopant source material which is represented by the precipitated species A_{ppt}, which in this diagram is assumed to be resulting from introducing the dopant into the semiconductor in supersaturated values and subsequently annealed for infinitely long times. When introduced in undersaturation (closed-system cases) the dopant will partition into neutral and ionized species according to the Fermi–Dirac distribution, but at a ratio differing from that at solubility case

dependent upon the formation Gibbs free energy of A^-. In their formulation [12], this free energy is an implicit function of a certain material's constants related to the semiconductor band structure.

The most straightforward way to illustrate the Fermi-level effect on $C^{eq}_{A^-}$ is via a derivation using the Fermi–Dirac distribution function. The mathematical procedure of treating the problem is the same as for partitioning the dopant into the neutral and ionized species for the closed system case. The physical condition imposed by the open system assumption is fairly different from that of the closed system case, and the dependence of $C^{eq}_{A^-}$ on p (which will be designated as p^{eq}) and on the semiconductor band structure constants will be explicit. Under the open-system assumption, the thermal equilibrium concentration of the neutral species, as given by

$$C^{eq}_{A^o} = C_o \exp\left(-\frac{g^f_{A^o}}{k_B T}\right) , \tag{2}$$

where C_o is the crystal lattice site density and $g^f_{A^o}$ is the Gibbs free energy of incorporating an A^o onto a lattice site, is constant at a given temperature, for two reasons. First, the source material is in principle inexhaustible. Second, because A^o is uncharged, $g^f_{A^o}$ is determined *chemically*, which is independent of the semiconductor doping type and level, i.e., it is independent of E_F. Furthermore, $g^f_{A^o}$ is also independent of any band-structure-related semiconductor constants.

For the ionized acceptor species A^-, the Fermi–Dirac distribution function is

$$f = \frac{1}{1 + g\exp\left(\frac{E_a - E^{eq}_F}{k_B T}\right)} , \tag{3}$$

where f is the fractional concentration of A^-, E_a is the shallow acceptor level energy position in the semiconductor bandgap, E^{eq}_F is the Fermi level energy position under thermal equilibrium conditions for the open system, k_B is Boltzmann's constant, T is the absolute temperature, and g is the hole degeneracy factor. In this paper, we adopt the convention that all semiconductor-band-related energies are measured relative to the vacuum level which is set at 0 eV. The quantity f specifies the fractional A^- concentration according to

$$f = \frac{C^{eq}_{A^-}}{C^{eq}_{A^o} + C^{eq}_{A^-}} . \tag{4}$$

Equations 3 and 4 yield *exactly*

$$C^{eq}_{A^-} = \frac{1}{g} C^{eq}_{A^o} \exp\left(\frac{E^{eq}_F - E_a}{k_B T}\right) . \tag{5}$$

As has already been mentioned, the solubility of the neutral acceptor species $C^{eq}_{A^o}$ is a unique constant at a given temperature, because of the open-system assumption. The open-system assumption can hold in experiments performed at high temperatures. In experiments with a pre-introduced total amount of acceptor atoms to begin with, for example, as obtained using the ion implantation process, the subsequent steady-state partition between the A^- and A^o species will also satisfy (5). However, now the eq notation, defined for the open system, no longer holds. This is because an E_F value differing from E^{eq}_F will be obtained. Noting that

$$E_a \approx E_v , \tag{6a}$$

$$n_i = N_v \exp\left(\frac{E_v - E_i}{k_B T}\right) , \tag{6b}$$

$$p^{eq} = N_v \exp\left(\frac{E_v - E^{eq}_F}{k_B T}\right) , \tag{6c}$$

where p^{eq} is the hole concentration under thermal equilibrium conditions, n_i is the intrinsic carrier concentration, E_v and E_i are respectively the valence band edge energy and the intrinsic Fermi-level energy, and N_v is the effective density of states of the valence band, (5) becomes

$$C^{eq}_{A^-} = \frac{1}{g} C^{eq}_{A^o}\left(\frac{N_v}{p^{eq}}\right) = \frac{1}{g} C^{eq}_{A^o}\left(\frac{n_i}{p^{eq}}\right)\exp\left(\frac{E_i - E_v}{k_B T}\right) . \tag{7}$$

The middle expression in (7) is of a more compact form, but the RHS expression is more useful for the practical reason that the values of n_i, E_i, and E_v are usually measured from experiments and are hence available for most semiconductors. In turn, p^{eq} satisfies the charge-neutrality condition

$$p^{eq} = \frac{1}{2}\left[C^{eq}_{A^-} + \sqrt{\left(C^{eq}_{A^-}\right)^2 + 4n_i^2}\right] \tag{8}$$

in the presence of only one shallow acceptor element.

It is seen from (7) and (8) that, for one shallow dopant species existing in a semiconductor alone, the thermal equilibrium concentration of the ionized species is dependent upon this concentration itself, since p^{eq} is determined by this concentration. With the exception of p^{eq}, all quantities in (7) are constants, and $C_{\mathrm{A^o}}^{\mathrm{eq}}$ is independent of n_{i} or any other semiconductor band-structure-related constants, for example, E_{i} or E_{v}, or the semiconductor doping type and level. These semiconductor band-structure-related constants will be different for different SL layers. Therefore, in the SL layers, $C_{\mathrm{A^-}}^{\mathrm{eq}}$ values will also be different, which leads to the A^- segregation phenomenon.

4 Charge-carrier concentrations at a heterojunction

In the immediate vicinity of a heterojunction, the electric charge-carrier concentration is different from those in the bulk of either of the two material layers forming the junction. Since the carrier concentration influences the junction region concentrations of $\mathrm{A_s^-}$ and I_{III}^{2+}, it influences also the $\mathrm{A_s^-}$ distribution in the SL. For a single semiconductor, an electric junction is formed if the dopant distribution is inhomogeneous, which can be due to an n- or p-type dopant alone or two dopants producing a p–n junction. For a SL structure, in addition to the effect of doping, the band gap discontinuity at the heterojunctions of the semiconductor layers will also contribute in producing the electric field. The band gap discontinuity contribution to the junction electric behavior can be particularly strong if the differences in the semiconductor band-structure constants are large.

The electric junction originates from the electric carrier thermal equilibrium property. Under thermal equilibrium conditions, the chemical potential of the charge carriers (or the Fermi level of electrons) is constant throughout the whole volume of the semiconductor or semiconductor structure. At the junction, this thermal equilibrium requirement produces a local depletion of carriers on one side of the junction and an accumulation of carriers on the other side of the junction. Thus, in a small region bordering the junction on one side, the carrier concentration becomes smaller than that in the bulk of the appropriate layer while in a small region on the other side of the junction the carrier concentration becomes larger than that in the bulk of the appropriate layer. The junction region is a space-charge region associated with local band bending. It consists of two neighboring sub-regions of opposite charges of the same total amount, producing an electric field confined primarily in the region. The charges may both be fixed charges associated with ionized dopant or host crystal atoms, or one may be of fixed charges while the other is of carriers, but never can both be carriers. The situation associated with doping of a single semiconductor is well known, and those for the heterostructure cases are schematically illustrated in Fig. 2.

In previous analyses [4–6] of dopant and self-atom diffusion profiles in AlGaAs/GaAs SL structures, the effect of the carrier concentrations at the heterojunctions has been ignored, for two reasons. First, the band-structure energy value differences between $\mathrm{Al}_x\mathrm{Ga}_{1-x}\mathrm{As}$ and GaAs are relatively small when compared to those involving other III-V materials, for example, those for the InP/InAs heterojunctions. The

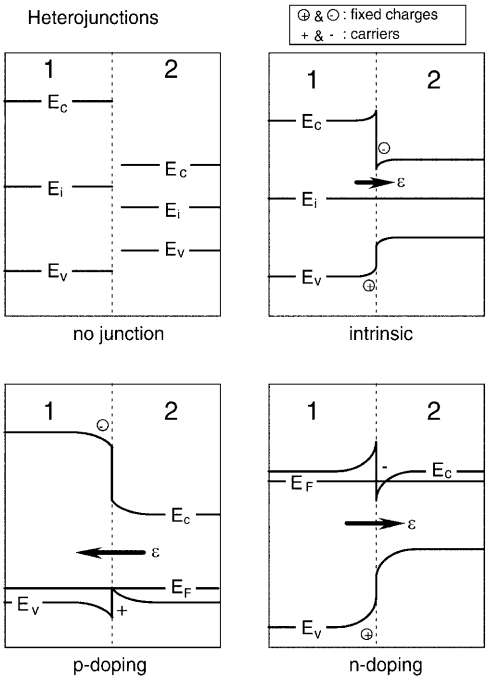

Fig. 2. A schematic diagram showing the band structure of III-V compounds forming a heterostructure, doped and undoped. Indicated are the band bending, the excess charges (fixed and carriers), and the junction electric field

band-structure-related energy values are shown in Fig. 3 for a number of III-V materials used in fabricating heterostructure devices. Second, for the involved $\mathrm{Al}_x\mathrm{Ga}_{1-x}\mathrm{As}$/GaAs experiments, the annealing temperatures were high and/or the annealing times were long, so that layer disordering or intermixing due to Al−Ga interdiffusion has occurred to a significant extent, which smears out the junction and hence also the effect of the junction carrier concentrations.

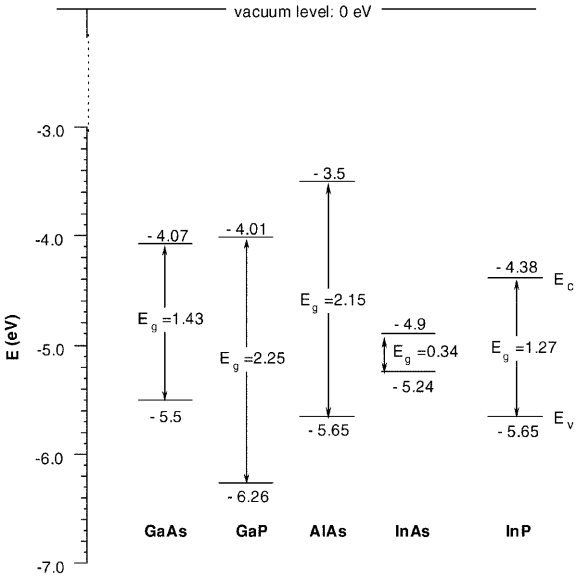

Fig. 3. Room-temperature III-V compound band-structure-related energies, E_{c}, E_{v}, and E_{g}. Values of E_{c} and E_{v} are those referenced to that of the vacuum level at 0 eV, and $E_{\mathrm{g}} = E_{\mathrm{c}} - E_{\mathrm{v}}$

Under static conditions at room temperature, the junction region carrier concentration, and hence also the associated electric field, is unchanging with time. There is no net carrier or current flowing, and the distribution of dopant atoms is also not changing with time. For III-V SL structure at elevated temperatures, however, the junction region carrier concentrations influence the local I_{III}^{2+} concentrations as well as the solubilities of A^-, which in turn affects the SL layer A^- concentrations.

5 Formulation of the acceptor distribution problem

The process of Zn^- or Be^- distribution in experiments involves diffusion and segregation of the electric carrier holes, the doubly-positively-charged group III self-interstitials I_{III}^{2+}, the ionized shallow acceptor atoms A^-, and an ionized interstitial species of the dopant atoms, the role of which is discussed shortly. Moreover, the junction-region carrier concentration changes with the electric field variations as a function of time and position.

The p-type dopants Zn and Be are substitutional–interstitial (A_s–A_i) species in GaAs and other III-V compounds. The thermal equilibrium concentration of A_s is much larger than that of A_i, and hence the measured Zn or Be concentration is that of A_s. The diffusion of A_s is accomplished by the migration of A_i and its subsequent change-over to become A_s, because the process is much faster than the migration of A_s atoms themselves via the vacancy mechanism. The A_i–A_s change-over process is governed by the kick-out mechanism involving [4–6]

$$A_i^+ \Leftrightarrow A_s^- + I_{III}^{2+} \,, \tag{9}$$

where the interstitial species of the dopant is assumed to be a donor, A_i^+.

To formulate the problem, we first account for the time and spatial variations in the concentrations of A_s^-, A_i^+, and I_{III}^{2+}, respectively designated as C_s, C_i, and C_I. In accordance with the discussion of the last paragraph, the change of C_s is described by

$$\frac{\partial C_s}{\partial t} = k_f C_i - k_b C_s C_I \,, \tag{10}$$

where k_f and k_b are, respectively, the forward and backward reaction constants associated with reaction (8). For the mobile species A_i^+ and I_{III}^{2+}, expressions obtained in previous formulation of Zn/Be diffusion [6] become insufficient, because inhomogenities of the thermal equilibrium concentrations of these species caused by the heterojunctions were not included. To account for both diffusion and segregation in the SL layers, the use of (1) in accordance with reaction (9) yields, respectively, for I_{III}^{2+} and A_i^+

$$\frac{\partial C_I}{\partial t} = \frac{\partial}{\partial x}\left[D_I \left(\frac{\partial C_I}{\partial x} - \frac{C_I}{C_I^{eq}} \frac{\partial C_I^{eq}}{\partial x} \right) \right] + \frac{\partial C_s}{\partial t} \,, \tag{11}$$

$$\frac{\partial C_i}{\partial t} = \frac{\partial}{\partial x}\left[D_i \left(\frac{\partial C_i}{\partial x} - \frac{C_i}{C_i^{eq}} \frac{\partial C_i^{eq}}{\partial x} \right) \right] - \frac{\partial C_s}{\partial t} \,, \tag{12}$$

where D_I and D_i are, respectively, the diffusivities of I_{III}^{2+} and A_i^+, which are constants at a given temperature in a given SL layer material.

We assume that *dynamical* equilibrium has been reached among the three species A_s^-, A_i^+, and I_{III}^{2+}, i.e., in (10) the left-hand side term $\partial C_s/\partial t$ is regarded as much smaller than either term on its RHS. This allows (10) to reduce to

$$\frac{C_i}{C_s C_I} = K \equiv \frac{C_i^{eq}}{C_s^{eq} C_I^{eq}} \,, \tag{13}$$

where $K = k_b/k_f$ is the equilibrium constant associated with reaction (9). The quantity C_s^{eq} is of the form of (7), i.e.,

$$C_s^{eq} = \frac{1}{g} C_{s^o}^{eq} \left(\frac{n_i}{p} \right) \exp\left(\frac{E_i - E_v}{k_B T} \right) \,, \tag{14}$$

with $C_{s^o}^{eq}$ being the thermal equilibrium concentration of the neutral acceptor atoms A_s^o.

For I_{III}^{2+}, one can assume either thermal equilibrium conditions hold or not. The assumption that thermal equilibrium conditions hold is applicable to [4, 6]: (i) the materials in the experiments are rich in group III elements, and/or (ii) the materials used in the experiments contain a sufficiently large density of sinks/sources for point defects of both the group III and the group V sublattices. The Zn indiffusion experiment of Weber et al. [8] was conducted at 550 °C without the use of an As over-pressure, which apparently satisfy the above condition (i). The experiments of Humer-Hager et al. [7] and of Häussler et al. [9] were performed using ion-implanted Be, which apparently satisfy the above condition (ii), because of the ion-implantation damage. Thus, we will use the assumption that thermal equilibrium conditions hold. This allows (11) to be replaced by

$$C_I = C_I^{eq} = C_I^{eq}(n_i) \left(\frac{p}{n_i} \right)^2 \,, \tag{15}$$

where $C_I^{eq}(n_i)$ is C_I^{eq} under intrinsic conditions which is independent of the crystal Fermi-level position or carrier concentrations.

Using (12)–(15), and noting that $C_s + C_i \approx C_s$ and hence $\partial(C_s + C_i)/\partial x \approx \partial C_s/\partial x$, we obtain

$$\begin{aligned} \frac{\partial C_s}{\partial t} &= \frac{\partial}{\partial x}\left[D_s^{eff} \left(\frac{\partial C_s}{\partial x} - \frac{C_s}{C_s^{eq}} \frac{\partial C_s^{eq}}{\partial x} \right) \right] \\ &= \frac{\partial}{\partial x}\left[D_s^{eff} \left(\frac{\partial C_s}{\partial x} + \frac{C_s}{p}\frac{\partial p}{\partial x} - \frac{C_s}{n_i}\frac{\partial n_i}{\partial x} \right.\right. \\ &\qquad \left.\left. - \frac{C_s}{k_B T}\left(\frac{\partial E_i}{\partial x} - \frac{\partial E_v}{\partial x} \right) - \frac{C_s}{C_{s^o}^{eq}} \frac{\partial C_{s^o}^{eq}}{\partial x} \right) \right] , \end{aligned} \tag{16}$$

where D_s^{eff} is the effective A_s^- diffusivity given by

$$D_s^{eff} = K C_I^{eq}(n_i) \left(\frac{p}{n_i} \right)^2 D_i \,, \tag{17}$$

which is the same as that describing Zn diffusion in GaAs [6].

The distribution of holes in the SL layers will be described by a generalized hole-transport equation including the hole segregation property in the different layers and the junction

electric field on the hole concentrations in the junction regions. With these effects included, in thermal equilibrium, the hole distribution in accordance with (6c) is

$$p^{\mathrm{eq}} = N_{\mathrm{v}} \exp\left(\frac{E_{\mathrm{v}} - E_{\mathrm{F}}^{\mathrm{eq}} - q\Phi}{k_{\mathrm{B}}T}\right) , \tag{18}$$

where q is the magnitude of the electron charge (taken to be positive); Φ is the electrostatic potential throughout the SL structure, which changes rapidly in the heterojunction regions; and $E_{\mathrm{F}}^{\mathrm{eq}}$ is the thermal equilibrium E_{F} position, which is constant throughout the SL structure. The quantities N_{v} and E_{v} are constants in each SL layer, but are different in the different SL layers. To account for the distribution of holes, the use of (1) and (18) yields

$$\frac{\partial p}{\partial t} = \frac{\partial}{\partial x}\left[D_p\left(\frac{\partial p}{\partial x} - \frac{p}{N_{\mathrm{v}}}\frac{\partial N_{\mathrm{v}}}{\partial x} - \frac{p}{k_{\mathrm{B}}T}\frac{\partial E_{\mathrm{v}}}{\partial x} + \frac{pq}{k_{\mathrm{B}}T}\frac{\partial \Phi}{\partial x}\right)\right] , \tag{19}$$

where D_p is the hole diffusivity. The band bending schematically shown in Fig. 1 result from the last three terms on the RHS of (19). The potential Φ satisfies Poisson's equation

$$\frac{\partial^2 \Phi}{\partial x^2} = \frac{q}{\varepsilon}\left[n - p + C_{\mathrm{A}^-} - C_{\mathrm{D}^+} - 2C_{\mathrm{I}}\right] , \tag{20}$$

where ε is the SL layer dielectric constant, C_{A^-} is the total ionized acceptor density for all acceptor species including $\mathrm{A_s^-}$, and C_{D^+} is the total ionized donor density. Here the quantities C_{A^-} and C_{D^+} are used in (20) to account also for predoping of the SL layers. In the absence of the electric field, (20) is just the charge-neutrality condition.

To obtain the distribution of A^- in the SL structure, (15)–(17), (19), and (20) need to be solved. In the SL structures the quantities n_{i}, E_{i}, E_{v}, N_{v}, and $C_{\mathrm{so}}^{\mathrm{eq}}$ are constants inside the bulk of each SL layer. However, these quantities change from layer to layer and hence their spatial derivatives become important in the heterojunction region.

6 Results and discussions

Some available experimental results [7–9] have been fitted using the present Fermi-level effect and junction carrier concentration effect model. Furthermore, some consequences of the model are discussed.

6.1 Fits of experimental results

Using the partial differential equation solver ZOMBIE [13], (15)–(17), (19), and (20) were numerically solved to fit the available experimental results [7–9], Figs. 4–6. In obtaining these fits, it is assumed that there is no intermixing of the SL layers, because in all cases the annealing time is sufficiently short and/or the temperature is sufficiently low, allowing the effect of layer intermixing to be ignored. It is also assumed that: (i) the dopant diffusivity value under intrinsic conditions, $D_{\mathrm{s}}^{\mathrm{eff}}(n_{\mathrm{i}})$, which is obtained by letting $p = n_{\mathrm{i}}$ in (16), is the same for all layers of a given SL structure; (ii) the $C_{\mathrm{I}}^{\mathrm{eq}}(n_{\mathrm{i}})$ value is the same for the different layers of each SL.

Figure 4 shows our calculated fitting curve together with the experimental results of Humer-Hager et al. [7] obtained by implanting Be into a $\mathrm{GaAs/Al_{0.3}Ga_{0.7}As}$ structure on a GaAs substrate and annealed at 860 °C for 3 s. It is seen from Fig. 3 that the fit is fairly satisfactory. The used Be intrinsic diffusivity value, $D_{\mathrm{s}}^{\mathrm{eff}}(n_{\mathrm{i}})$, is $1 \times 10^{-13}\,\mathrm{cm^2\,s^{-1}}$, and the used self-interstitial thermal equilibrium concentration under intrinsic conditions, $C_{\mathrm{I}}^{\mathrm{eq}}(n_{\mathrm{i}})$, is $3.65 \times 10^{11}\,\mathrm{cm^{-3}}$. In the experiment [7], the SL layers were pre-doped. The predoping conditions are listed in Table 1. Also listed in Table 1 are the used values of the materials' band-structure-related constants, including n_{i}, E_{i}, E_{v}, and N_{v} of each material layer,

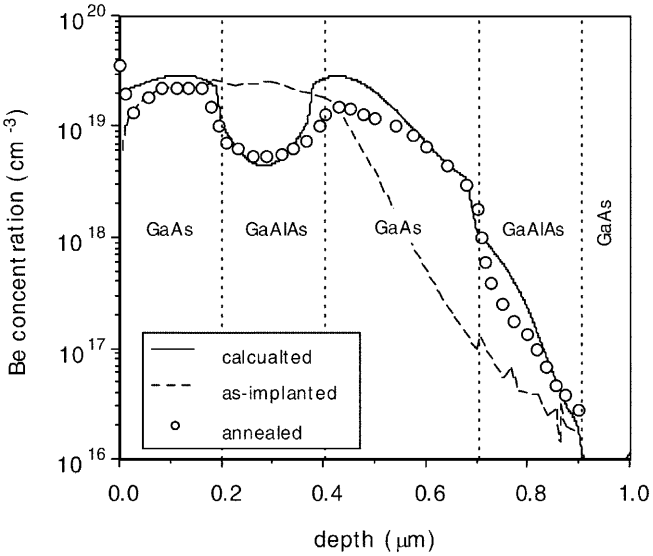

Fig. 4. The Be data of Humer-Hager et al. [7] in GaAs/AlGaAs SL obtained by ion implantation, together with the calculated fitting curve. The *broken line* is the as-implanted Be profile, the symbols are the Be data after annealing, and the *solid line* is the fitting curve

Table 1. SL layer pre-doping conditions of the experiment of Humer-Hager et al. [7], and materials' constants used for obtaining the fit. The values of n_{i}, E_{i}, E_{v}, and N_{v} are those at the experimental temperature of 860 °C, referenced to the vacuum level of 0 eV. The listed GaAs $m_{\mathrm{so}}^{\mathrm{eq}}$ value is with respect to the $\mathrm{Al_{0.3}Ga_{0.7}As}$ $C_{\mathrm{so}}^{\mathrm{eq}}$ layer value

Layer	pre-doping type/ concentration /$\mathrm{cm^{-3}}$	n_{i} /$\mathrm{cm^{-3}}$	E_{i} /eV	E_{v} /eV	N_{v} /$\mathrm{cm^{-3}}$	$m_{\mathrm{so}}^{\mathrm{eq}}$
GaAs	$\mathrm{n^+/2 \times 10^{18}}$ (0.1 μm) $\mathrm{n\ /2 \times 10^{17}}$ (0.1 μm)	7.65×10^{16}	−4.85	−5.5	6.02×10^{19}	12
$\mathrm{Al_{0.3}Ga_{0.7}As}$	$\mathrm{n\ /2 \times 10^{17}}$	2.83×10^{16}	−4.86	−5.629	7.85×10^{19}	1
GaAs	$\mathrm{p\ /3 \times 10^{18}}$	7.65×10^{16}	−4.85	−5.5	6.02×10^{19}	12
$\mathrm{Al_{0.3}Ga_{0.7}As}$	$\mathrm{n\ /2 \times 10^{17}}$	2.83×10^{16}	−4.86	−5.629	7.85×10^{19}	1
GaAs	$\mathrm{n^-/5 \times 10^{16}}$	7.65×10^{16}	−4.85	−5.5	6.02×10^{19}	12

Table 2. SL layer pre-doping conditions of the experiment of Weber et al. [8], and materials' constants used for obtaining the fit. The values of n_i, E_i, E_v and N_v are those at the experimental temperature of 550 °C, referenced to the vacuum level of 0 eV. The listed layer m_{so}^{eq} values are with respect to the InP layer C_{so}^{eq} value.

Layer	pre-doping type/ concentration /cm^{-3}	n_i /cm^{-3}	E_i /eV	E_v /eV	N_v /cm^{-3}	C_{so}^{eq}
InGaAs	$n^+/3\times10^{19}$	2.2×10^{16}	−4.8	−5.31	8.67×10^{19}	100
InP	$n/3\times10^{17}$	1.5×10^{16}	−5.2	−5.65	2×10^{19}	1
InGaAsP	$p/3\times10^{17}$	3.24×10^{16}	−4.95	−5.43	5.17×10^{19}	35
InP	$n/3\times10^{17}$	1.5×10^{16}	−5.2	−5.65	2×10^{19}	1

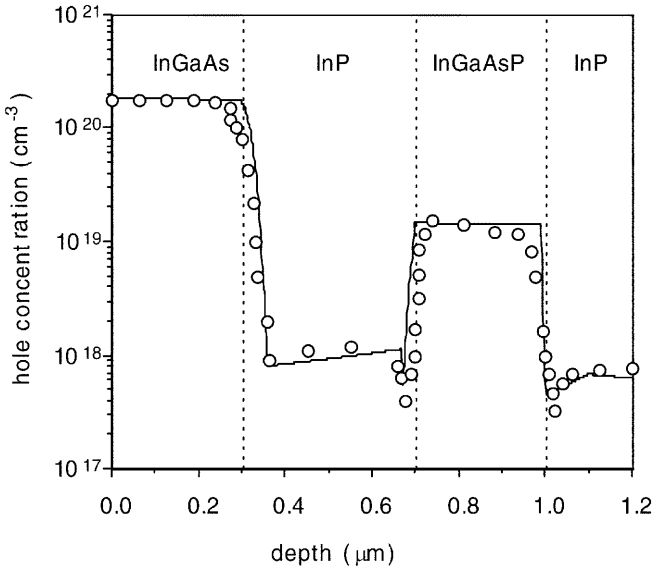

Fig. 5. The hole data (*open circles*) in an InGaAs/InP/InGaAsP/InP SL obtained by Weber et al. [8] using Zn indiffusion, together with the calculated fitting curve (*solid line*)

and the relative C_{so}^{eq} values among the layers. The values of the materials' band-structure-related constants are those appropriate for the diffusion temperature of 860 °C, which are not directly available from the literature. The procedure of obtaining such high temperature values is a complex one discussed elsewhere [14].

Figure 5 shows our calculated fitting curve together with the experimental results of Weber et al. [8] obtained by measuring hole concentrations after diffusing Zn at 550 °C for 12 min into an InGaAs/InP/InGaAsP/InP SL. It is seen that the fit is excellent. For this case, our calculated Zn profile (not shown) is nearly identical to that of the holes. The used Zn intrinsic diffusivity value $D_s^{eff}(n_i)$ is 3×10^{-13} cm^2 s^{-1}, and the used intrinsic self-interstitial thermal equilibrium concentration value $C_I^{eq}(n_i)$ is 5×10^9 cm^{-3}. The $D_s^{eff}(n_i)$ and $C_I^{eq}(n_i)$ values are in accordance with those used by Zimmermann et al. [15]. The SL layer pre-doping conditions [8] are listed in Table 2, together with the used values of the materials' constants for obtaining the fit.

Figure 6 shows two examples of our fits to the experimental data of Häussler et al. [9], from which it is seen that the fits are excellent. They obtained four sets of results by implanting Be into InP/InGaAs structures and annealing at 850 °C for 6 or 26 s, two with the implanted Be peak concentration at the layer interface, and two with the Be peak inside the InGaAs layer. Those shown in Fig. 5 are the two latter cases. The degree of satisfaction of our fits to all four sets of their data are the same. For these cases [9], the used

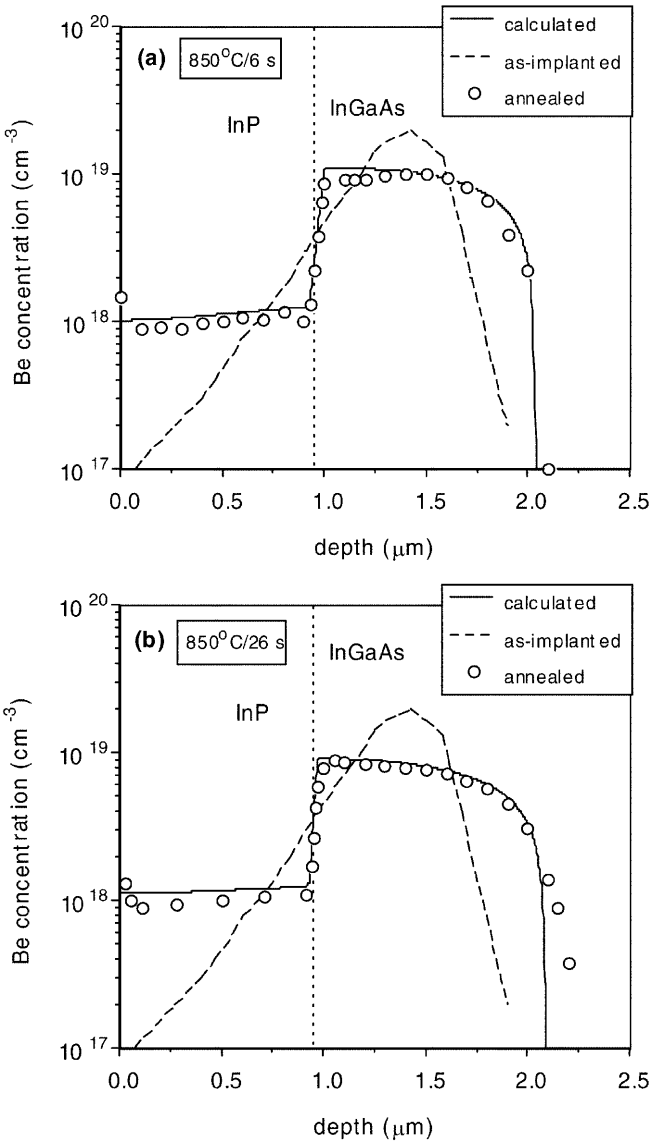

Fig. 6a,b. The Be data of Häussler et al. [9] with Be implanted into the InGaAs layer and annealed at 850 °C for **a** 6 s, and **b** 26 s. *Dashed lines* are the as-implanted data, *open circles* are those after annealing, and the *solid lines* are the calculated fitting curves

Be intrinsic diffusivity value $D_s^{eff}(n_i)$ is 2.1×10^{-13} cm^2 s^{-1} and the intrinsic self-interstitial thermal equilibrium concentration value $C_I^{eq}(n_i)$ is 3.7×10^{11} cm^{-3}. The used values of the materials' constants for obtaining the fits are listed in Table 3. The SL layer pre-doping conditions [9] are not known and we have assumed that they are intrinsic to begin with.

Table 3. SL layer nature of the experiment of Häussler et al. [9], and SL materials' constants used for obtaining the fit. The values of n_i, E_i, E_v, and N_v are those at the experimental temperature of 850 °C, referenced to the vacuum level of 0 eV. The listed $In_{0.47}Ga_{0.53}As$ layer $m_{s^o}^{eq}$ value is with respect to the InP layer $C_{s^o}^{eq}$ value.

Layer	pre-doping type/ concentration /cm^{-3}	n_i /cm^{-3}	E_i /eV	E_v /eV	N_v /cm^{-3}	$C_{s^o}^{eq}$
$In_{0.47}Ga_{0.53}As$	unknown	8×10^{17}	−4.936	−5.35	1×10^{20}	8.1
InP	unknown	6×10^{16}	−5.18	−5.65	3.2×10^{19}	1

6.2 *The segregation phenomenon*

The most outstanding feature of the shallow acceptor distribution data shown in Figs. 4–6 is the segregation of dopants in the adjacent SL layers to a sizable magnitude. Our fittings to these data, consequently, are simultaneous descriptions of the acceptor diffusion and segregation processes. The main features of our treatment of the segregation process can be more clearly understood by an examination of the steady-state segregation phenomenon. For two adjacent SL layer materials α and β, the thermal equilibrium segregation coefficient of an ionized shallow acceptor species is obtained from (7) as

$$\begin{aligned} m_{A^-}^{eq}(\alpha,\beta) &= \frac{C_s^{eq}(\alpha)}{C_s^{eq}(\beta)} \\ &= m_{A^o}^{eq}\frac{n_i(\alpha)}{n_i(\beta)}\frac{p^{eq}(\beta)}{p^{eq}(\alpha)} \\ &\quad\times\exp\left(-\frac{E_i(\alpha)-E_v(\alpha)-E_i(\beta)+E_v(\beta)}{k_BT}\right). \end{aligned} \tag{21}$$

In (21) the thermal equilibrium hole concentrations $p^{eq}(\alpha)$ and $p^{eq}(\beta)$ satisfy the charge neutrality conditions

$$p^{eq}(\alpha)=\frac{1}{2}\left[C_s^{eq}(\alpha)+\sqrt{\left(C_s^{eq}(\alpha)\right)^2+4n_i^2(\alpha)}\right], \tag{22a}$$

$$p^{eq}(\beta)=\frac{1}{2}\left[C_s^{eq}(\beta)+\sqrt{\left(C_s^{eq}(\beta)\right)^2+4n_i^2(\beta)}\right], \tag{22b}$$

when the concentrations of I_{III}^{2+} and other dopant species are assumed to be small. Moreover, $m_{A^o}^{eq}$ in (21) is the thermal equilibrium segregation coefficient of the neutral acceptor species given by

$$m_{A^o}^{eq}(\alpha,\beta)=\frac{C_{s^o}^{eq}(\alpha)}{C_{s^o}^{eq}(\beta)}=\exp\left(-\frac{g_{A^o}^{f}(\alpha)-g_{A^o}^{f}(\beta)}{k_BT}\right). \tag{23}$$

The quantity $m_{A^o}^{eq}(\alpha,\beta)$ is constant at a given temperature, because, as has been mentioned before, $g_{A^o}^{f}(\alpha)$ is determined *chemically*, which is independent of the semiconductor charge-carrier type and concentrations. On the other hand, it is seen from (21) that the thermal equilibrium segregation coefficient of A^-, $m_{A^-}^{eq}(\alpha,\beta)$, is further dependent upon the charges in the semiconductor structure.

In practice, an acceptor species may be introduced into a SL at concentration levels different from its solubility value, and its distribution in the SL layers will reach a steady state for long annealing times. For such cases, (7) still applies. For the neutral acceptor species,

$$m_{A^o}(\alpha,\beta)=\frac{C_{s^o}(\alpha)}{C_{s^o}(\beta)}=\frac{C_{s^o}^{eq}(\alpha)}{C_{s^o}^{eq}(\beta)}=m_{A^o}^{eq}(\alpha,\beta), \tag{24}$$

obtains. For the ionized acceptor species,

$$\begin{aligned} m_{A^-}(\alpha,\beta) &= \frac{C_s(\alpha)}{C_s(\beta)} \\ &= m_{A^o}^{eq}\frac{n_i(\alpha)}{n_i(\beta)}\frac{p(\beta)}{p(\alpha)} \\ &\quad\times\exp\left(-\frac{E_i(\alpha)-E_v(\alpha)-E_i(\beta)+E_v(\beta)}{k_BT}\right) \end{aligned} \tag{25}$$

obtains.

An outstanding aspect of (25) is that

$$m_{A^-}(\alpha,\beta)\neq m_{A^-}^{eq}(\alpha,\beta), \tag{26}$$

because the quantity $p(\beta)/p(\alpha)$ is not equal to $p^{eq}(\beta)/p^{eq}(\alpha)$. In (25), $p(\alpha)$ and $p(\beta)$ satisfy (22) provided the 'eq' designation is removed. Another outstanding aspect is that $m_{A^-}(\alpha,\beta)$ is dependent upon the doping level. Knowing either the total acceptor dose or the acceptor concentration in either layer, (25) can be solved. The former condition applies to the cases shown in Figs. 4 and 6 for which a given dose of Be has been introduced into the sample by ion implantation, and the latter condition applies to cases resembling that shown in Fig. 5, for which Zn is diffused into the SL using an external source material, if it is not the unique equilibrium source material which determines the Zn solubility values in the SL. In fact, since the Zn source material used by Weber et al. is $ZnAs_2$ [8] for obtaining the results shown in Fig. 5, it is not the thermal equilibrium source material because the InP layers contain no As atoms. There are two limiting cases of (25). For sufficiently low doping conditions for which $p\approx n_i$ holds in both materials, (25) reduces to

$$\begin{aligned} m_{A^-}(\alpha,\beta) &= m_{A^o}(\alpha,\beta) \\ &\quad\times\exp\left[\frac{E_i(\alpha)-E_v(\alpha)-E_i(\beta)+E_v(\beta)}{k_BT}\right], \end{aligned} \tag{27}$$

while for sufficiently high doping conditions for which the self-doping condition $p\approx C_s$ holds in both materials, (25) reduces to

$$\begin{aligned} m_{A^-}(\alpha,\beta) &= \left[m_{A^o}(\alpha,\beta)\frac{n_i(\alpha)}{n_i(\beta)}\right]^{\frac{1}{2}} \\ &\quad\times\exp\left[\frac{E_i(\alpha)-E_v(\alpha)-E_i(\beta)+E_v(\beta)}{2k_BT}\right]. \end{aligned} \tag{28}$$

As an example, Fig. 7 shows the calculated steady-state segregation coefficient of Zn^- between the first two layers of materials of the case shown in Fig. 5. The materials involved are InGaAs and InP, and the results are given as a function of Zn concentration in InP.

Equation 25 is also obtained from integrating (16) by noting that in steady state the C_s flux vanishes. Thus, our

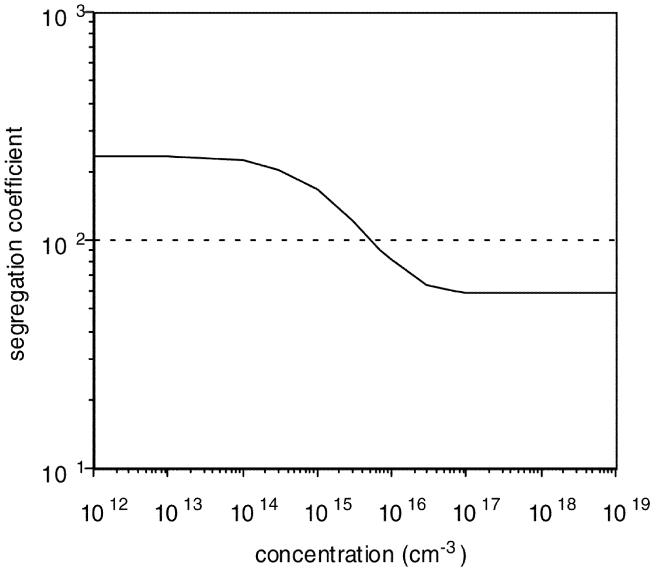

Fig. 7. Calculated steady-state Zn segregation coefficient in the bulk of the first two layers of materials of the example shown in Fig. 5, i.e., InGaAs and InP. The InP layer Zn concentration is used as the independent variable. The *dashed line* is *the chemically* determined part, which is strictly valid only for the neutral Zn atoms. The *solid line* is that of ionized Zn, which is determined chemically as well as by the Fermi-level effect

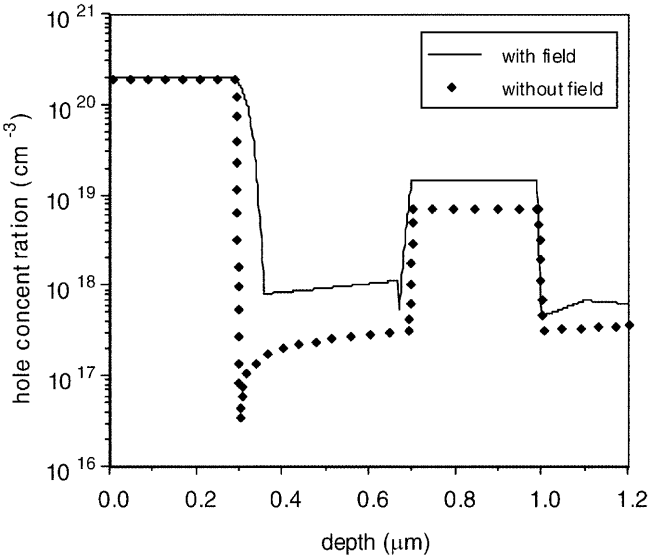

Fig. 8. Calculated results for fitting the experimental data of Weber et al. [8] shown in Fig. 5, with and without the inclusion of the junction carrier concentration effect (or junction electric field effect). The results with the junction carrier concentration effect included fit the experimental data well, see Fig. 4. The results without the junction carrier concentration effect included do not fit the experimental data: the Zn indiffusion process is too slow

formulation of the present problem is consistent with the thermodynamic definitions of the involved quantities.

6.3 Role of the junction carrier concentrations

The heterojunction carrier concentration influences the concentrations of A_s^- and of I_{III}^{2+}, and hence also the A_s^- distribution rate throughout the SL. Since the junction and hence also its electric property physically exist, in general, the effect should be taken into account. However, to avoid the complexity involved, to ignore this effect seems to be a common practice. We believe that whether this effect can be ignored is dependent upon the nature of the problem. The effect should have played a minor role in long-time high-temperature experiments, but a significant role in low-temperature and/or short-time experiments. In general, it will not be a prudent approach to just ignore this effect.

The junction carrier concentration effect has been found to be fairly large for the Zn indiffusion case shown in Fig. 5. Figure 8 shows the calculated results with and without including this effect. The latter results are obtained by letting $\partial\Phi/\partial x = 0$ in (19) and $\partial^2\Phi/\partial x^2 = 0$ in (20), which simply amounts to the use of the charge-neutrality condition throughout the SL structure. From Fig. 8, it is seen that, without including the junction carrier concentration (or junction field) effect, the A_s^- concentrations in the three buried layers, InP, InGaAlP, and InP, are significantly lower than those in the case of including the effect. Physically, this outcome is understood by noting that the hole thermal equilibrium concentrations in the InGaAs and InGaAsP layers are larger than those in the InP layers by orders of magnitude. During the A_s^- distribution process, one rate-limiting factor is the A_s^- fluxes across a heterojunction. Without including the junction-region hole concentration effect, the flux is controlled by a relatively small hole concentration that is the same as that in the InP layer bulk. In the presence of junction-region hole concentration effect, the junction flux becomes much larger because at the junction region on the InP side there is a hole accumulation, resulting in a hole concentration that is much larger than that in the InP layer bulk on an order of magnitude basis. Meanwhile, also on an order-of-magnitude basis, the depletion of holes on the InGaAs or InGaAsP sides of the appropriate junctions is not too significant, because the bulk hole concentrations in these layers are orders of magnitude larger than those in the adjacent InP layers.

6.4 Previous attempts

It appears that there exist three prior attempts in modeling the acceptor diffusion–segregation phenomenon [8, 16, 17], to various degrees of satisfaction in fitting the experimental data.

In the first attempt, Weber et al. [8] provided a simulation of their own experimental data, those shown in Fig. 5, by assuming that the solubilities in the layers of the InGaAs/InP/InGaP/InP structure are of different constant values. By diffusing Zn into individual InGaAs and InP materials at 550 °C, they found an 80 times Zn solubility difference. Their analysis provided a rough approximation to the complicated situation, in the sense that the effect of factor $m_{s^o}^{eq}$ has been in principal accounted for, but the Fermi-level effect contribution to $m_{s^-}^{eq}$ was ignored.

The second attempt is that of Bracht et al. [16], who fitted the experimental data shown in the present Figs. 4–6 approximately by assuming a constant dopant solubility difference in the SL layers due to an *electronic* effect given by $\exp(-\delta\varepsilon/k_BT)$, where $\delta\varepsilon$ is the E_v difference of two adjacent SL layers. This means that $m_{s^o}^{eq}$ is taken to be 1 among the layers. Their electronic effect is arrived at via a Fermi-level

stabilization energy (E_{FS}) argument, which bears a resemblance to the presently discussed Fermi-level effect model. We believe that the Fermi-level stabilization energy concept is inherently illusive and difficult to understand. Furthermore, from the presently used $m_{s^o}^{eq}$ values listed in Tables 1–3 all of which do not equal to 1, it is most probable that the attempt is physically incorrect.

The third attempt concerns our own preliminary effort [17]. Irrespective of the apparently satisfactory fits obtained, which are very close to the present ones, the report contained errors. First, the segregation effect was attributed to the junction electric field effect alone, which is incorrect. Second, in what should have been the present (16), the terms concerning the role of n_i and of C_{s^o} were missing. The missing of the n_i term was accidental and in the actual calculation the effect was included. The missing of the C_{s^o} term is due to the use of the assumption $m_{s^o}^{eq} = 1$. In obtaining the fits, the effect of $m_{s^o}^{eq}$ does not equal to 1 was compensated by an adjustment in the E_v value differences among the adjacent layers. This is possible because, in (16), E_i, E_v, and C_{s^o} constitute *similarity* terms in the sense that they are of an identical mathematical form. It is obvious that the mathematical forms of the E_i and E_v terms in (16) are identical. By noting that $C_{s^o}^{eq}$ is given by (2), the term $\left(\partial C_{s^o}^{eq}/\partial x\right)/C_{s^o}^{eq}$ in (16) is equal to $-\left(\partial g_{A^o}^{f}/\partial x\right)/(k_B T)$, which is also of an identical mathematical form of that of the E_i and E_v terms. Thus, since the values of E_i, E_v, $g_{A^o}^{f}$ and their differences are all of the order of a couple to a few eV, it is seen that the misuse of the value of one quantity can be readily compensated by using also a wrong value for another quantity. This means that, to solve the problem, we need to know the values of E_i, E_v, and $C_{s^o}^{eq}$ accurately, or else a fitting to the experimental data can be obtained by accounting for the effects of these quantities by an arbitrary value for any one of the three or in any combination, which can result in an erroneous interpretation of the physics involved. Under the $m_{s^o}^{eq} = 1$ assumption, our previous fitting parameters for the InGaAs and InP layers of Fig. 5 will lead to unacceptable E_i values that are too close to the E_c values of the appropriate layer materials. Thus, presently, the $m_{s^o}^{eq} = 1$ assumption is abandoned. The presently used materials' constants and $m_{s^o}^{eq}$ values given in Tables 1–3 are judged to be reasonable, but it is almost certain that their accuracies can be further improved when more band energy information becomes available for these materials. Since the assumption of Bracht et al. [16] also involves $m_{s^o}^{eq} = 1$, we suppose that the same situation will hold also for their attempt.

From the values given in Tables 1–3, it is seen that the segregation coefficient of the neutral acceptor species A^o, $m_{s^o}^{eq}$, determines the order of magnitude of the observed segregation phenomenon. The Fermi-level effect and the junction carrier concentration effect determine the fine details of the observed acceptor distributions, including the profile shapes and a deviation of the segregation magnitude many times from that described by $m_{s^o}^{eq}$ alone.

7 Conclusions

In conclusion, we mention that the observed p-dopant segregation behavior in SL layers in short annealing time and/or low annealing temperature experiments has been satisfactorily explained using a model incorporating three effects. The overall dopant segregation behavior results from the chemical effect on the neutral acceptor species thermal equilibrium concentrations, the Fermi-level effect on ionized acceptor and charged point defect concentrations, and the junction carrier-concentration effect on the dopant distribution kinetics in the SL layers. In principle, in SL layers of different chemical compositions the diffusivities of the ionized dopant atoms should be different. The present satisfactory fits of the experimental data means that, quantitatively, the contribution of this factor to the observed dopant segregation phenomenon is fairly small. This Fermi-level effect model has also provided satisfactory fits to available boron distribution profiles in Ge_xSi_{1-x}/Si heterostructures, see the accompanying article [1], and its application to a number of n-type doping effects in a variety of semiconductor heterostructures will be reported shortly [2].

References

1. C.-H. Chen, U.M. Gösele, T.Y. Tan: Appl. Phys. A, **68**, 19 (1999)
2. C.-H. Chen, U.M. Gösele, T.Y. Tan: Appl. Phys. A, to be submitted
3. D.G. Deppe, N. Holonyak Jr.: J. Appl. Phys. **64**, R93 (1988)
4. T.Y. Tan, U. Gösele, S. Yu: Crit. Rev. Solid State Mater. Sci. **17**, 47 (1991)
5. T.Y. Tan, U. Gösele: Appl. Phys. Lett. **52**, 1240 (1988)
6. S. Yu, T.Y. Tan, U.M. Gösele: J. Appl. Phys. **69**, 3547 (1991)
7. T. Humer-Hager, R. Treichler, P. Wurzinger, H. Tews, P. Zwicknagl: J. Appl. Phys. **66**, 181 (1989)
8. R. Weber, A. Paraskevopoulos, H. Schroeter-Janssen, H.G. Bach: J. Electrochem. Soc. **138**, 2812 (1991)
9. W. Häussler, J.W. Walter, J. Müller: In Ion Beam Processing of Advanced Electronic Materials, ed. by N.W. Cheung, A.D. Marwick, J.B. Roberto, Proc. Mat. Res. Soc. Symp. Vol. 147 (Mat. Res. Soc., Pittsburgh, PA 1989) p. 333
10. C.-H. Chen, U. Gösele, T.Y. Tan: In Semiconductor Process and Device Performance Modeling, ed. by J.S. Nelson, C.D. Wilson, S.T. Dunham (1997 Mater. Res. Soc. Fall Meeting, Symposium Q, Boston, Dec. 1-5, 1997). In press
11. H.-M. You, U.M. Gösele, T.Y. Tan: J. Appl. Phys. **74**, 2461 (1993)
12. S. Yu, U.M. Gösele, T.Y. Tan: J. Appl. Phys. **69**, 3547 (1991)
13. W. Jüngling, P. Pichler, S. Selberherr, E. Guerrero, H.W. Pötzl: IEEE Trans. Electron Devices **ED-32**, 156 (1985)
14. C.-H. Chen: Ph.D. thesis, Duke University (available: December 1998)
15. H. Zimmermann, U. Gösele, T.Y. Tan: J. Appl. Phys. **73**, 150 (1993)
16. H. Bracht, W. Walukiewicz, E.E. Haller: In Semiconductor Process and Device Performance Modeling, ed. by J.S. Nelson, C.D. Wilson, S.T. Dunham (1997 Mater. Res. Soc. Fall Meeting, Symposium Q, Boston, Dec. 1-5, 1997). In press
17. T.Y. Tan, C.-H. Chen, U. Gösele, R. Scholz: In Diffusison Mechanisms in Crystalline Materials, ed. by C.R.A. Catlow, N. Cowern, D. Farkas, Y. Mishin, G. Vogl, Proc. Mat. Res. Soc. Vol. 527 (Mater. Res. Soc., Pittsburgh, PA 1998) p. 321